Shock Waves (2013) 23:299–306
DOI 10.1007/s00193-012-0378-7

ORIGINAL ARTICLE

Flow visualization of supersonic laminar flow over a backward-facing step via NPLS

Z. Chen · S.H. Yi · L.F. Tian · L. He · Y.Z. Zhu

Received: 19 October 2011 / Revised: 1 April 2012 / Accepted: 30 April 2012 / Published online: 18 May 2012

Abstract An experimental study on a supersonic laminar flow over a backward-facing step of 5 mm height was undertaken in a low-noise indraft wind tunnel. To investigate the fine structures of $Ma = 3.0$ and 3.8 laminar flow over a backward-facing step, nanotracer planar laser scattering was adopted for flow visualization. Flow structures, including supersonic laminar boundary layer, separation, reattachment, redeveloping turbulent boundary layer, expansion wave fan and reattachment shock, were revealed in the transient flow fields. In the $Ma = 3.0$ BFS (backward-facing step) flow, by measuring four typical regions, it could be found that the emergence of weak shock waves was related to the K–H (Kelvin–Helmholtz) vortex which appeared in the free shear layer and that the convergence of these waves into a reattachment shock was distinct. Based on large numbers of measurements, the structure of time-averaging flow field could be gained. Reattachment occurred at the location downstream from the step, about 7–7.5 h distance. After reattachment, the recovery boundary layer developed into turbulence quickly and its thickness increased at an angle of 4.6°. At the location of $X = 14h$, the redeveloping boundary layer was about ten times thicker than its original thickness, but it still had not changed into fully developed turbulence. However, in the $Ma = 3.8$ flow, the emergence of weak shock waves could be seen seldom, due to the decrease of expansion. The reattachment point was thought to be near $X = 15h$ according to the averaging result. The reattachment shock was not legible, which meant the expansion and compression effects were not intensive.

Keywords NPLS · Flow visualization · Supersonic · Backward-facing step

Communicated by K. Kontis.

The paper was based on work that was presented at the 28th International Symposium on Shock Waves, 17–22 July 2011, Manchester, UK.

Z. Chen (✉) · S.H. Yi · L.F. Tian · L. He · Y.Z. Zhu
College of Aerospace and Material Engineering,
National University of Defense Technology, Changsha, China
e-mail: gfkdchenzhi@163.com

1 Introduction

Flow separation and reattachment caused by sudden geometric changes are well known. The importance of such flows to engines, such as lifetime and reliability, has been stressed in many publications. Actually, a two-dimensional backward-facing step (BFS) has received attention owing to its geometrical simplicity [1]. In the past several decades, there were large numbers of studies on the mechanism of separated and reattaching flows experimentally and numerically. To study flow structures by flow visualization, techniques such as schlieren, shadow, interference and numerical methods, have been usually adopted. Shen and Ma [2] used WBIV (Whitelight bubble image velocimetry) to measure the structures of starting vortices and found four stages in this process. Akiko and Masahiko [3] studied the supersonic flow over BFS with a normal injection using the numerical method and shadow technique, and found that fierce reaction between injection and recirculation region was distinct. Schram et al. [4] studied the eddy structures shed in a BFS flow. Particle image velocimetry (PIV) measurements were performed in the recirculating region located downstream of the step. An automatic vortex detection algorithm was developed for the purpose of the automatic analysis of the experimental data to detect and characterize the eddy structures [4]. Fadai-Ghotbi et al. [5] performed URANS (Unsteady

Reynolds-Averaged Navier–Stokes) and EBRSM (Elliptic Blending Reynolds Stress Model) to reproduce the vortex shedding behind a BFS and investigate the amplitude of the energy of the resolved eddies. However, traditional flow visualization techniques such as schlieren, shadow and interference encountering problems of integral effects and low spatial resolution, are not competent for measuring the complicated structures of high-speed turbulent flow which required high spatiotemporal resolution. NPLS, developed by the research group consisting of the authors, is a new flow visualization technique for measuring fine structures of supersonic flow. Its spatial resolution can reach the micron scale with a time resolution of 6 ns, and the temporal correlation resolution can reach 0.2 μs. Its high spatiotemporal resolution and high SNR (signal-to-noise ratio) make it an excellent tool for studying characteristics of supersonic flows [6]. In recent years, NPLS has been proposed by Yi and coworkers [6] and it has been used in studies on supersonic mixing layer [7,8], aero-optical effects [9] and supersonic flat-plate boundary layer [10].

Attention is given to fine flow structures of supersonic laminar flow over a BFS at $Ma = 3.0$ and $Ma = 3.8$ in this paper. The whole flow-field structures and fine structures of four typical regions are revealed, respectively, via NPLS. By performing a time-averaging process, the transient and time-averaging flow-field structures are also studied and analyzed. The effect of Mach number in BFS flows is also studied by changing the nozzle to generate different flow fields.

2 Experimental facilities and NPLS measurements

2.1 NPLS

As shown in Fig. 1, it is the NPLS testing system that is used in this paper. A dual-cavity Nd:YAG pulsed laser is used as its light source, which emits two laser beams of 6 ns pulse width according to the scheduling set by the synchronizer. A light sheet of less than 1 mm thick illuminates the flow field of interest. Owning to the excellent following ability, nanoparticles with the nominal diameter of 20 nm can catch the complicated structures in supersonic flow field and scatter laser light effectively to generate high SNR images. The recording system is an interline transfer double exposure CCD whose resolution is 2K × 2K and the shortest interval of double exposure is 0.2 μs. The synchronizer, whose accuracy is 250 ps, can adjust the time of laser emitting and CCD exposure according to the signal of computer to make sure that the two laser beams are exposed in the frames of dual exposure, respectively. The computer's charges set the parameters of the synchronizer, storing and processing images [6–8]. Based on NPLS, several new testing techniques have been developed. One of them is a new density testing technique, named NPLS-DT (NPLS-Density Testing), developed by Tian using an oblique shock wave calibration [9]. Performance of NPLS in complex flow field is shown in Fig. 2. More details of NPLS such as particle dynamic behavior, response analysis of particle, light scattering characteristic of nanoparticles and validation of this system can be found in [6].

2.2 Supersonic wind tunnel and the testing model

The experiments were carried out in an indraft low-noise wind tunnel which can generate $Ma = 3.0$ and $Ma = 3.8$ supersonic flow field by changing the nozzle, as shown in Fig. 3. The total pressure and stagnation temperature of the incoming flow were $P_0 = 1$ atm and $T_0 = 300$ K, respectively. The size of the cross section of the testing section was 100 mm × 120 mm. High-quality optical glass for imaging was enchased in its four sides. Table 1 lists the parameters of the wind tunnel. Figure 4 shows the step height of the testing model h was 5 mm, while the spanwise length of the step d was 120 mm. Table 2 shows the distance between the wall upstream from the step and the ceiling of the testing chamber H was 80 mm. These parameters ensured $d/H \geq 10$ and the expansion ratio $E_r = 1.067$, making the flow be considered as two dimensional. The Reynolds number of the $Ma = 3.0$ incoming flow R_h, based on the step height, was 3.85×10^4, while it was 2.6×10^4 for the $Ma = 3.8$ flow as shown in Table 3.

3 Results and discussion

3.1 Flow structures

Figure 5 shows the NPLS images of the $Ma = 3.0$ transient flow field, which distinctly reveals structures of the whole flow field. According to the text above, it is obvious that this high SNR image is generated by gathering the light scattered by the tracing particles in the testing flow field, whose flow following ability is excellent. Thus, structures of flat plate boundary layer, recirculation region, free shear layer, redeveloping turbulent boundary layer, weak shock waves, reattachment shock and expansion wave fan can be seen clearly. As shown in Fig. 5, supersonic laminar boundary layer forms on the wall upstream from the step and its thickness increases slowly along the streamwise direction. After the supersonic flow passes over the step, it accelerates while its density decreases because of the sudden geometric expansion of the wall and the impact from the expansion waves. The region of expansion waves in Fig. 5 looks darker than the incoming flow. A free shear layer is formed between the separated flow and the recirculation region at the step corner. Several weak shock waves which converge into a reattachment shock downstream are thought to be induced by the K–H vortex in the free shear layer. Reattachment occurs somewhere

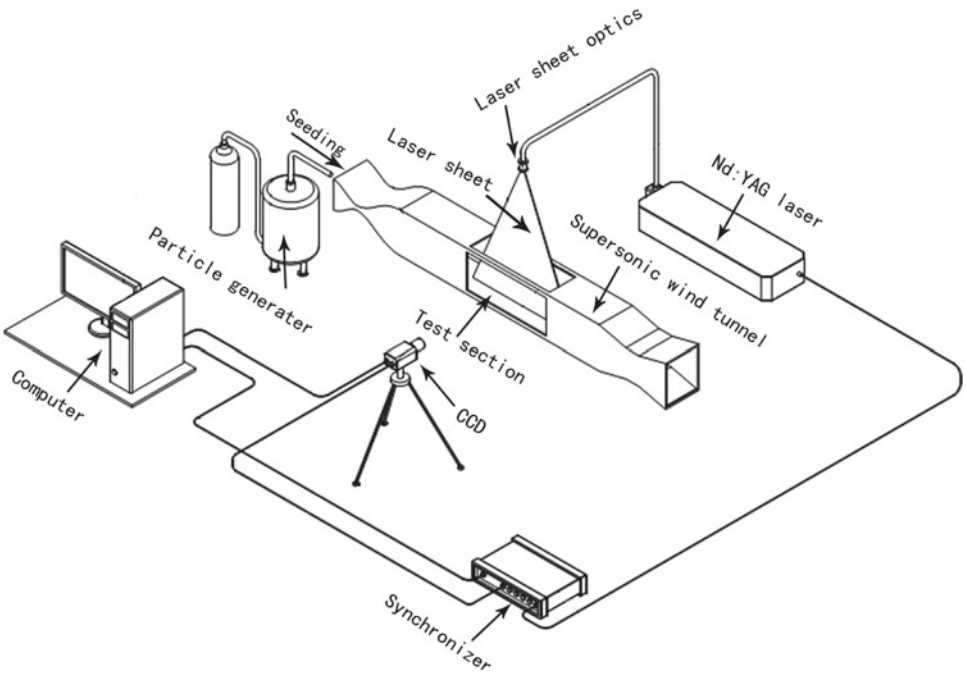

Fig. 1 Scheme of NPLS

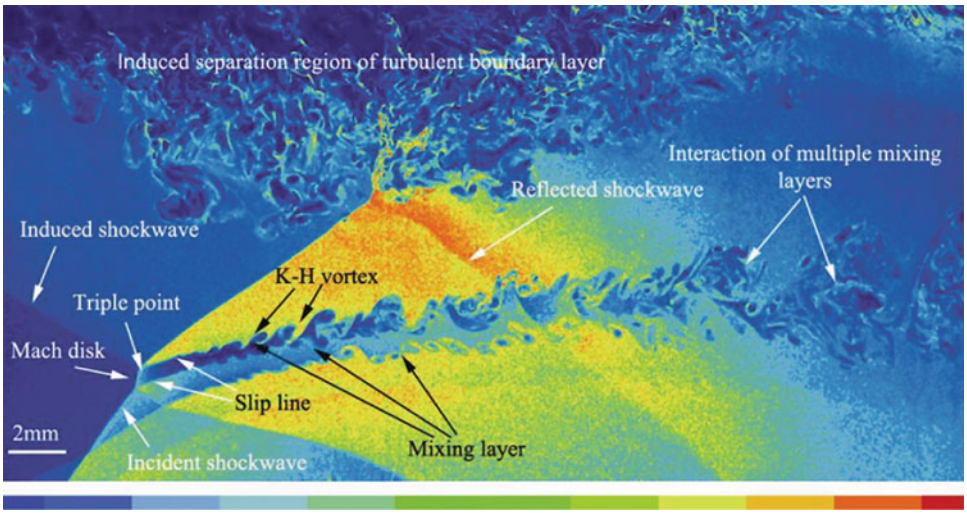

Fig. 2 NPLS image of a complex supersonic flow

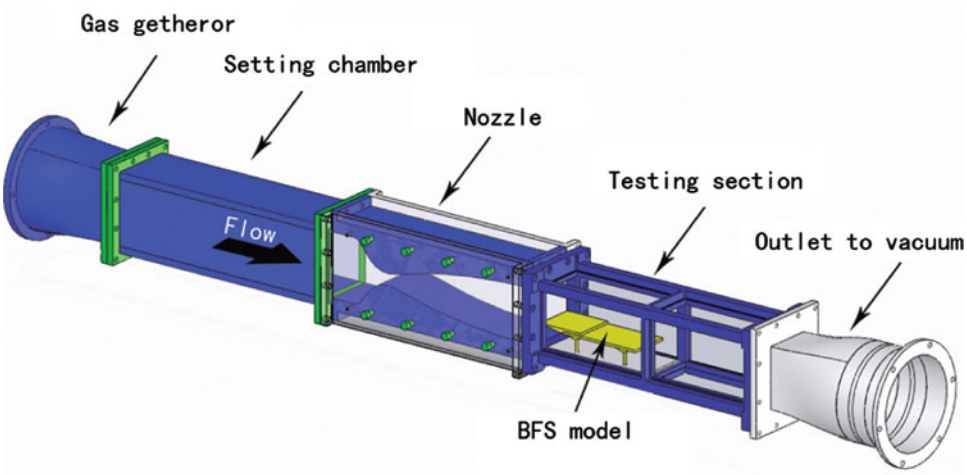

Fig. 3 Low-noise indraft supersonic wind tunnel

Table 1 List of symbols

BFS	Backward facing step
NPLS	Nano-tracer planar laser scattering
K–H	Kelvin–Helmholtz
WBIV	Whitelight bubble image velocimetry
H	Height of step
D	Spanwise length of the step
H	Distance between the step and the ceiling of the test section
E_r	Expansion ratio, $H/(H-h)$
PIV	Particle image velocimetry
URANS	Unsteady Reynolds-averaged Navier–Stokes
EBRSM	Elliptic blending Reynolds stress model
NPLS-DT	NPLS-density testing
SNR	Signal-to-noise ratio
$R_h = \frac{\rho v h}{\mu}$	Reynolds number of the incoming flow based on the step height

Table 2 Parameters of wind tunnel

	Case 1	Case 2
Ma	3.0	3.8
P_0 (MPa)	0.1	0.1
T_0 (K)	300	300
P (Pa)	2,750	874.3
T (K)	107	77.2
ρ (kg/m^3)	0.089	0.039
a (m/s)	207.5	176.1
U (m/s)	622.5	669.3
μ (N s/m^2)	7.43×10^{-6}	5.09×10^{-6}
R_e	7.49×10^{-6}	5.19×10^{-6}
t_{running} (s)	$\geq$10	$\geq$10

Table 3 Parameters of the 2D BFS testing model

h	d	d/h	H
5 mm	120 mm	24	80 mm
R_h= rvh/u	$E_r = H/(H-h)$		
3.85×10^4 ($Ma = 3.0$)	1.067		
2.6×10^4 ($Ma = 3.8$)			

downstream, generating a recirculation region between the reattachment point and the step. Because of the low flow density in the recirculation region with few nanoparticles, this recirculation region also looks dark in Fig. 5. By repeating measurements and performing an averaging process, large numbers of instantaneous flow-field images could be gained along with a time-averaging flow field, as shown in Fig. 6. Though some transient characters are blotted out in the averaging process, the main characters are revealed in the time-averaging flow field. The angle of expansion waves is 25.5° as Arrowhead A points out, showing the expansion effect. The angle of averaging reattachment shock is 13.4°, as shown by Arrowhead B, which indicates the compression effect. After reattachment, the recovery boundary layer develops quickly with an angle of 4.6° according to its averaging profile as Arrowhead D shows, from which we would know how the new boundary layer develops.

Flow structures of $Ma = 3.8$ BFS flow at various times are revealed, as shown in Fig. 7. Four typical flow fields are selected which can represent the basic features of this flow pattern. The K–H vortex without the emergence of weak shock waves still can be seen at the location where the arrowheads point to. The long length of the recirculation region shows that the impact from the step in the $Ma = 3.8$ flow is not as intense as it is on the $Ma = 3.0$ flow. The time-averaging flow field of the $Ma = 3.8$ BFS flow is revealed in Fig. 8. The angle of expansion waves as the Arrowhead A points out is 16.6°, while the angle of reattachment shock is about 11.7°, pointed out by Arrowhead B. Though waves reflected by the ceiling of the testing section emerge in the flow field as revealed by Arrowhead C, it can hardly influence the BFS flow structures which locate upstream. Arrowhead D shows that the angle at which the redeveloping boundary layer increases is 3.8°. Thus, by comparing these two BFS flows, it can be concluded that with the increasing Mach

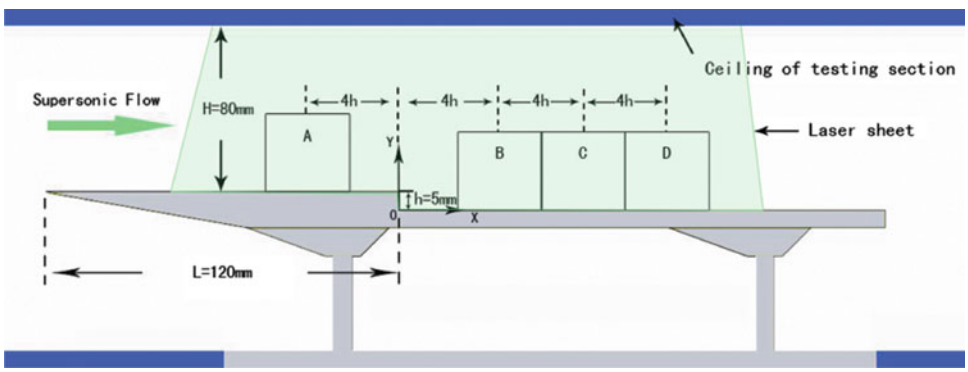

Fig. 4 Flow geometry and measuring regions for the supersonic BFS flow

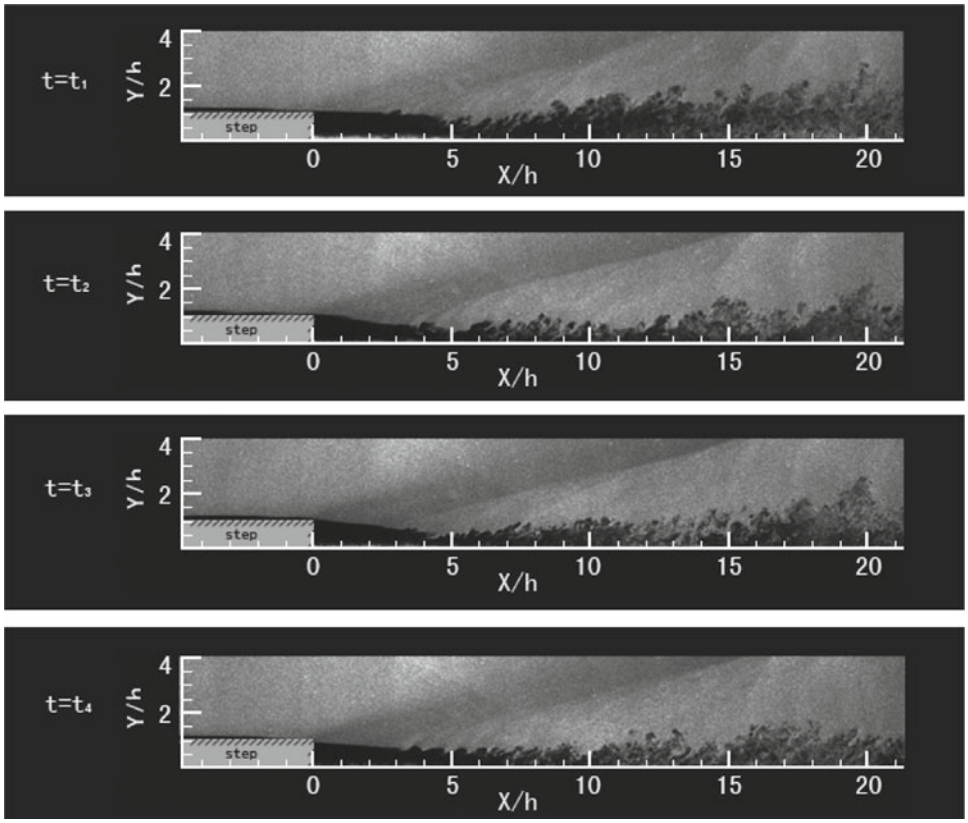

Fig. 5 Transient flow structures of the $Ma = 3.0$ BFS flow at different time

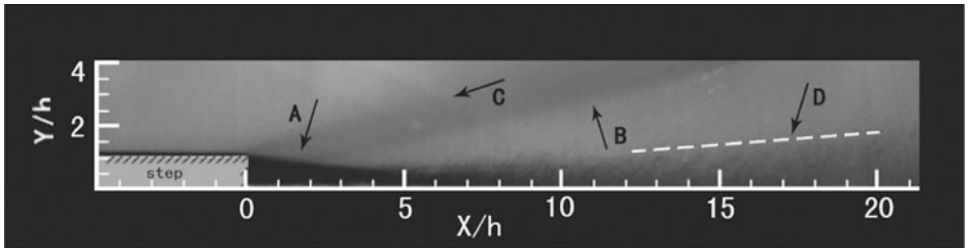

Fig. 6 Time-averaging flow field of the $Ma = 3.0$ BFS flow

number, the recirculation region becomes longer, while the expansion effect of the step and the compression effect of the lower wall downstream of the step are weakened. The location where the reattached boundary layer changes into turbulent boundary layer is believed to be at $X = 15h$ in the $Ma = 3.8$ BFS flow, while this phenomenon occurs in the $Ma = 3.0$ BFS flow at around $X = 7h$.

3.2 Fine flow structures of four typical regions in the $Ma = 3.0$ flow field

To study this typical flow further, four regions are selected and named A, B, C and D, as shown in Fig. 4. Region A is located $4h$ upstream from the step where the supersonic boundary layer is the main structure and impacts the other three regions downstream. The aim of measuring this region is to compare with former studies and to supply with the incoming boundary condition for CFD. The center of Region B is located $4h$ downstream from the step. This region contains the most complicated structures which are the key points in studies on BFS flow. As for Region C, it is located 8h downstream from the step. The importance of this region is to determine the reattachment point and the length of reattachment region. The last Region D is moved $4h$ downstream from Region C, where the recovery effect of the new developed boundary layer is concerned. Flow structures of these regions are shown in Figs. 9, 10, 11 and 12, respectively. Figure 9 reveals the fine structure of supersonic laminar boundary layer, which is formed on the flat wall surface upstream from the step. The boundary layer develops slowly and stably without any distinct structures and its thickness is about $0.1h$. Because of its low density, the boundary layer contains less nanoparticles than the main flow field, and thus it looks dark on the image. As the most complicated region, Fig. 10 depicts structures such as recirculation region, free shear layer and weak shock waves. Figure 10 shows that

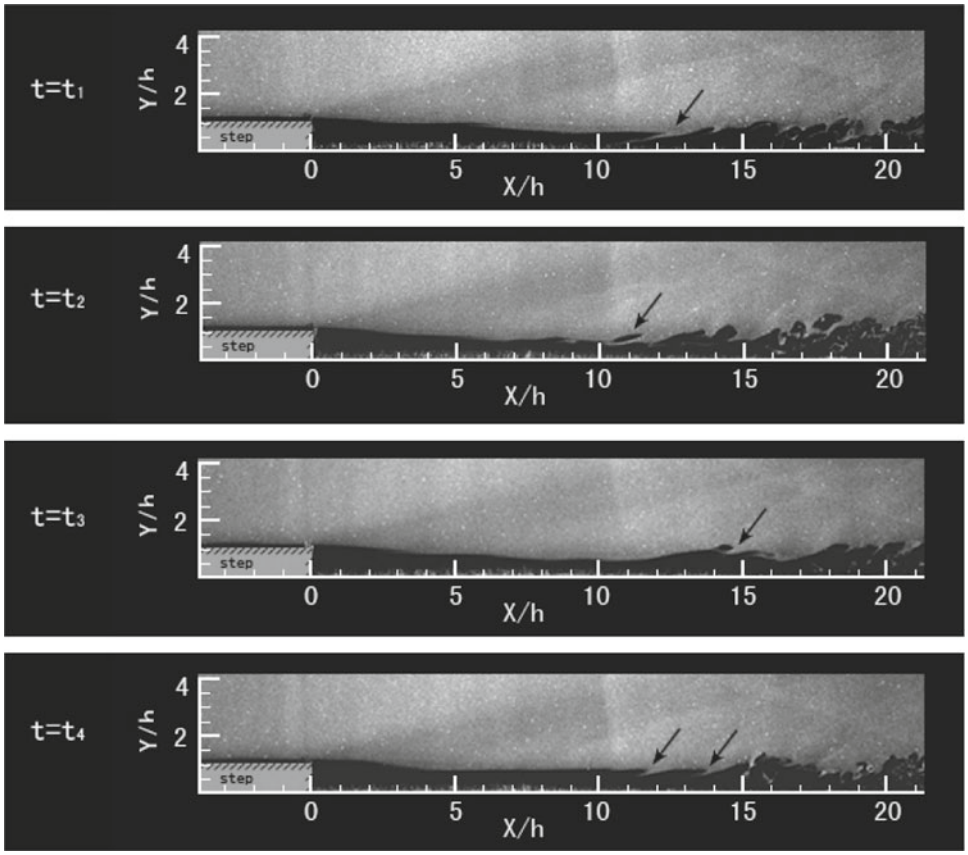

Fig. 7 Transient flow structures of the $Ma = 3.8$ BFS flow at different time

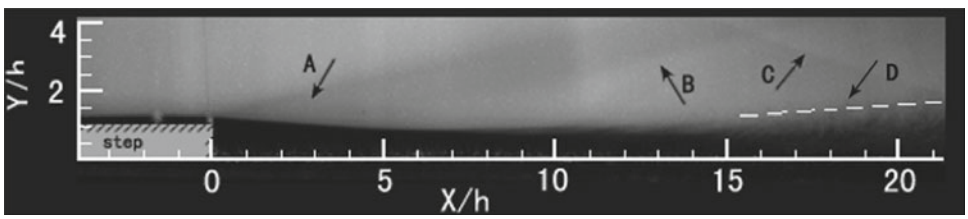

Fig. 8 Time-averaging flow field of the $Ma = 3.8$ BFS flow

the reattachment point is not located in this region and the length of the recirculation region is at least more than $6h$. The outline of free shear layer is like a saw tooth, which is the typical structure of K–H vortex that is thought to be the cause of the emergence of the weak shock waves. In addition, the intensity of the weak shock waves is not strong in this region, because the distinction of the brightness before and after the weak shock waves is not evident. Besides free shear layer and weak shock waves, new boundary layer and reattachment shock emerge in Fig. 11. Reattachment occurs in this region around the location of $7h$ downstream from the step. It is obvious that the free shear layer inclines to the flat wall and after reattachment a new boundary layer forms and develops. Comparing Figs. 9 with 11, we would find that the former laminar boundary layer changes into turbulence after separation and reattachment immediately. Obviously, the turbulent boundary layer does not develop fully. Weak shock waves in this region converge, forming the so-called reattachment shock. Figure 12 shows the last testing region and the main feature is the recovery of the new boundary layer. Although the new boundary layer has not changed to fully developed turbulence, in fact it develops quickly. In Fig. 12, the thickness of the boundary layer at $X = 10h$ is about $0.5h$, while at $X = 14h$ it increases to $1h$ with an averaging angle, as discussed above. Also in Fig. 12 it can be seen that waves from the upside wall of the test section interferes into the testing region, but only influences the flow field downstream. In addition, the reattachment shock becomes more intensive in this region.

4 Conclusions

NPLS, as a flow visualization technique, is newly developed for supersonic turbulence testing with high spatiotemporal resolution. It uses nanoparticles as tracer and can visualize

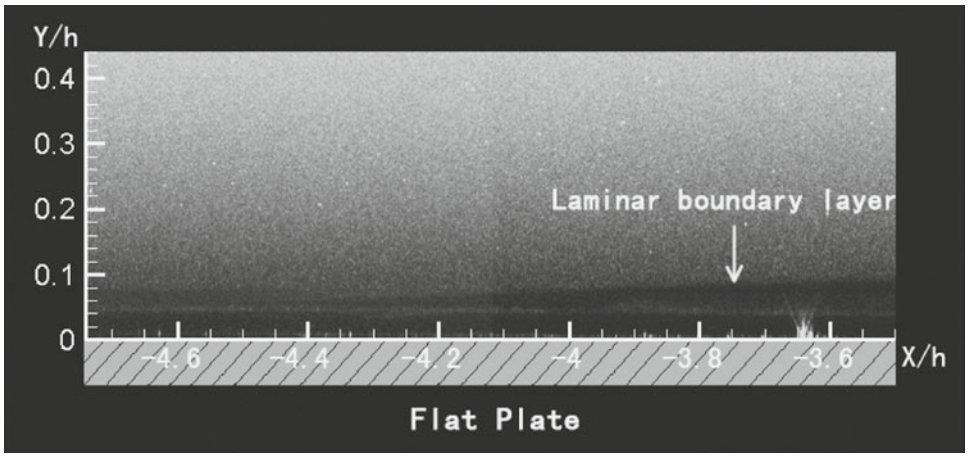

Fig. 9 Boundary layer upstream from the step in the $Ma = 3.0$ BFS flow, corresponding to Region A in Fig. 4

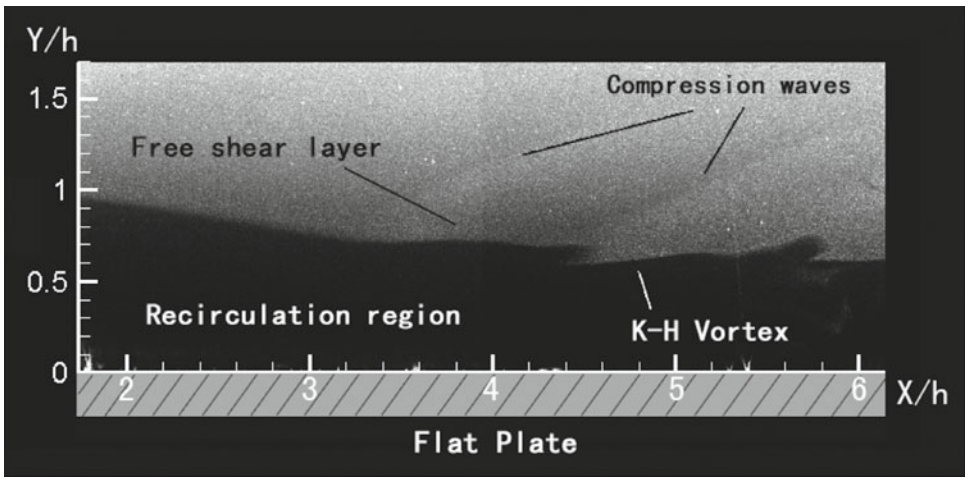

Fig. 10 Flow structures around the recirculation region in the $Ma = 3.0$ BFS flow, corresponding to Region B in Fig. 4

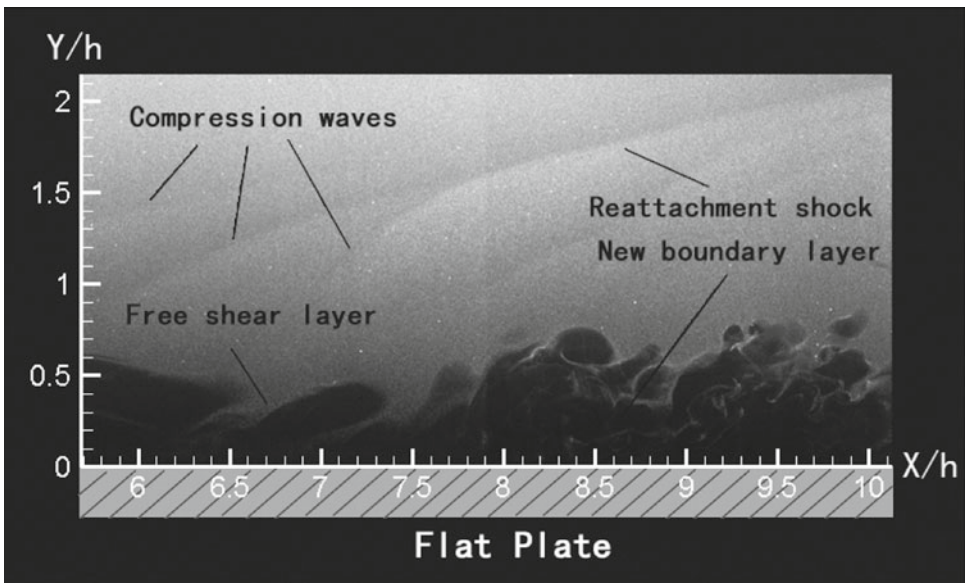

Fig. 11 Flow structures around the reattachment region in the $Ma = 3.0$ BFS flow, corresponding to Region C in Fig. 4

transient structures of a cross section of supersonic 3D flow field at a time resolution of 6 ns, and a temporal correlation resolution of 0.2 μs. In this paper, NPLS is adopted to visualize the flow structure of the supersonic laminar flow over a BFS at $Ma = 3.0$ and $Ma = 3.8$. The whole flowfield structures are revealed in NPLS images, which include supersonic boundary layer upstream from the step, recirculation region and shearing layer caused by the separation,

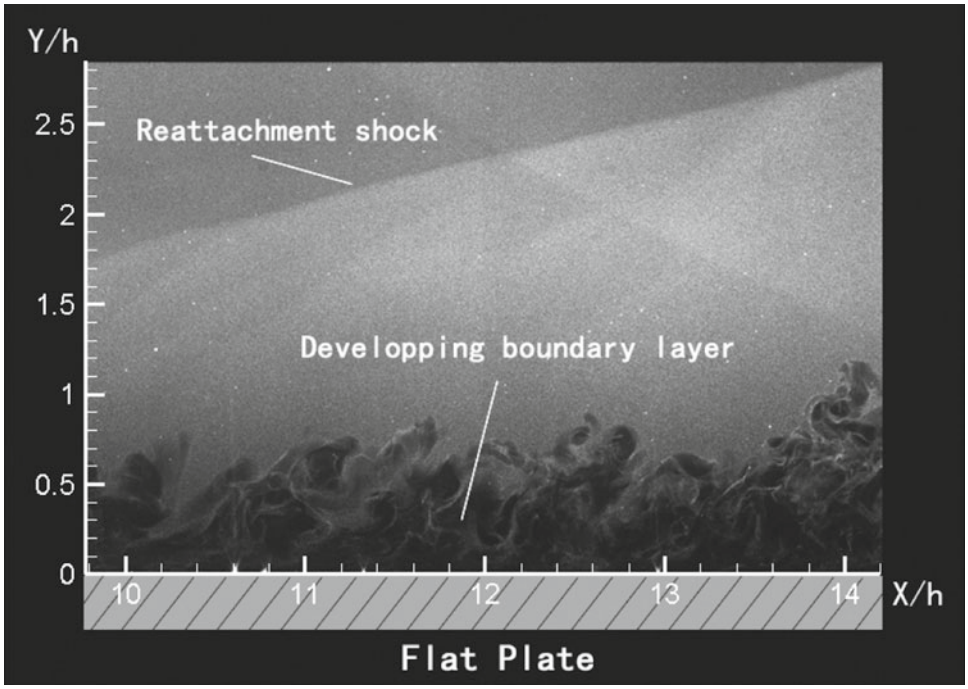

Fig. 12 Flow structures of the recovery region in the $Ma = 3.0$ BFS flow, corresponding to Region D in Fig. 4

weak shock waves, reattachment shock and so on. Transient and time-averaging flow fields are displayed, showing different characters of the flow. Four regions are measured and discussed, respectively, and the results reveal the fine flow structures and features of these regions. In addition, it is thought that the emergence of weak shock waves is related to the K–H vortex in the free shear layer. Due to the effect of increasing Mach number, in the $Ma = 3.8$ BFS flow, the length of recirculation region augments, while the angle of expansion waves and reattachment shock decrease. The K–H vortex does not appear with the weak shock waves in pairs.

Acknowledgments This work was supported by the National Basic Research Program of China under Grant Nos.2009 CB724100 and The National Natural Science Foundation of China under Grant No.11172326.

References

1. Hall, S.D., Behnia, M., Fletcher, C.A.J., Morrisonl, G.L.: Investigation of the secondary corner vortex in a benchmark turbulent backward-facing step using cross-correlation particle imaging velocimetry. Exp. Fluids **35**(2), 139–151 (2003)
2. Shen, G.X., Ma, G.Y.: The investigation on the properties and structures of starting vortex flow past a back-ward facing step by WBIV technique. Exp. Fluids **21**(1), 57–65 (1996)
3. Akiko, M., Masahiko, M.: Flow structure of supersonic flow past backward-facing step with perpendicular injector. AIAA-98-0939
4. Schram, C., Rambaud, P., Riethmuller, M.L.: Wavelet based eddy structure eduction from a backward facing step flow investigated using particle image velocimetry. Exp. Fluids **36**(2), 233–245 (2004)
5. Fadai-Ghotbi, A., Manceau, R., Boree, J.: Revisiting URANS computations of the backward-facing step flow using second moment closures. Influence of the numerics. Flow Turbulence Combust **81**, 395–414 (2008)
6. Zhao, Y.X., Yi, S.H., Tian, L.F., Cheng, Z.Y.: Supersonic flow imaging via nanoparticles. Sci. China E: Technol. Sci. J. **52**(12), 3640–3648 (2009)
7. Zhao, Y.X., Yi, S.H., Tian, L.F., Cheng, Z.Y.: Density field measurement and approximate reconstruction of supersonic mixing layer. Chin. Sci. Bull. J. **55**(19), 2004–2009 (2010)
8. Yi, S.H., He, L., Zhao, Y.X., Tian, L.F., Cheng, Z.Y.: A flow control study of a supersonic mixing layer via NPLS. Sci. China G: Phys. Mech. Astron. J. **52**(12), 2001–2006 (2009)
9. Tian, L.F., Yi, S.H., Zhao, Y.X., He, L., Cheng, Z.Y.: Study of density field measurement based on NPLS technique in supersonic flow. Sci. China G: J. **52**(9), 1357–1363 (2009)
10. He, L., Yi, S.H., Zhao, Y.X., Tian, L.F., Chen, Z.: Visualization of coherent structures in a supersonic flat-plate boundary layer. Chin. Sci. Bull. J. **56**(6), 489–494 (2011)